# Machine Learning Identification of Experimental Conditions for the Synthesis of Single-phase White Phosphors

Hailong Yuan, Romain Génois, Estelle Glais, Fei Chen, Qiang Shen, Lianmeng Zhang, Eric Faulques, Luyuan Qi, Florian Massuyeau, Romain Gautier

# Machine Learning Identification of Experimental Conditions for the Synthesis of Single-phase White Phosphors

Hailong Yuan,[a],[b] Romain Génois,[b] Estelle Glais,[b] Fei Chen,[a] Qiang Shen,[a] Lianmeng Zhang,[a] Eric Faulques,[b] Luyuan Qi,[c] Florian Massuyeau,[b] and Romain Gautier* [b]

[a] State Key Lab of Advanced Technology for Materials Synthesis and Processing, Wuhan University of Technology, Wuhan 430070, China.
[b] Centre National de la Recherche Scientifique (CNRS), IMN, 2 rue de la Houssinière, 44322 Nantes, France.
[c] Certara, 54 Rue de Londres, 75008 Paris, France.

*Corresponding author, Email: Romain.Gautier@cnrs-imn.fr

**SUMMARY:** Single-phase white phosphors for solid-state lighting are commonly designed using different dopants responsible of emissions in different spectral regions. However, phenomena of energy transfers and concentration quenching often prevent any clear prediction of the accurate experimental conditions to be selected, leading to a time-consuming trial-and-error discovery process. In this research article, a high-throughput (HT) experimental approach equipped with machine learning (ML) enabling an efficient identification of the experimental conditions for designing a white phosphor is demonstrated. $Li_2BaSiO_4$:Eu,Ce was selected to illustrate this strategy. 88 samples were prepared from the initial synthesis of eight compounds with different amounts of Eu and Ce dopants followed by a post-treatment under a gradient of temperature. The decision tree model, based on the experimental data of 88 samples, identified the experimental conditions to design a white emission, i.e., the material should be prepared under a reducing atmosphere with a ratio of dopants [Eu]/([Ce]+[Eu]) between 0.17 and 0.83 followed by an oxidation under air at a temperature between 628 °C and 673 °C. The analysis of the experimental conditions to obtain other colors of emission (i.e. bluish purple, pink, orange, green or yellow/green), which were also identified by ML, enabled to rationalize the different mechanisms of energy transfers between dopants.

## INTRODUCTION

As a new generation of lighting source, white light emitting diodes (wLEDs) are focusing the researchers' and industrials' attentions due to high energy savings and a fast growing market.[1–4] One of the most common methods to produce wLEDs is to combine a blue-emitting LED chip with a yellow phosphor such as $Y_3Al_5O_{12}:Ce^{3+}$ (YAG:Ce).[5,6] However, the color rendering index (CRI) of such wLEDs is poor due to the lack of a red component which limits the application in higher-end products.[7,8] Adding a red phosphor or combining UV chips with three primary phosphors (red, green and blue phosphors) have been reported to improve the color rendering, while preserving performances.[9–11] However, the reabsorption between different phosphors, the different particle sizes or nonuniformity of luminescence properties when used in wLEDs remain important issues.[9,10,12] For these reasons, single-phase white emitting phosphors have attracted increasing attention in the past years.[13,14]

The most common approach to design a single-phase white emitting phosphor is to dope a host with multiple dopants.[15–17] For some compounds, the combination of two dopants can lead to a white emission.[18] However, in order to cover all the visible region (380 nm ~740 nm) and obtain a good color rendering of the white emission, more than two dopants, which exhibit different emission wavelengths, are commonly necessary.[10,15] In this case, phenomena such as energy transfers (ET) between these dopants are difficult to predict, and make the balance of the emissions and the generation of a white light challenging. [17,19] In this research article, we demonstrate how machine learning (ML) can be used to predict the emission color of a host with multiple dopants and to identify the appropriate experimental conditions for synthesizing single-phase white phosphors. As representative datasets (i.e. both positive and negative outcomes) are needed for ML techniques,[20–22] a high-throughput (HT) experimental approach has been developed to synthesize large amounts of materials with different concentrations of dopants. This HT approach uses the ability of several dopants such as Mn or Eu to exhibit different emissions according to their oxidation states.[19,23–26] The strategy consists in firstly synthesizing a few materials codoped with different amounts of two dopants. Then, an oxidation step under a gradient of temperature is carried out to tune the oxidation states of dopants and the resulting emissions. Thus, a relatively large library of compounds with different concentrations of dopants and different oxidation states ratio of these dopants can be obtained and analyzed using ML models.

## RESULTS AND DISCUSSION

$Li_2BaSiO_4$ (LBSO) doped with Eu and Ce was selected to illustrate the proposed approach. In LBSO, the two oxidation states of Europium ($Eu^{2+}$ and $Eu^{3+}$) commonly lead to different emissions in the same host.[27–30] $Eu^{2+}$ presents a green emission (Figure S1). This emission, which originates from the 4f-5d transitions, strongly depends on the ions environment (symmetry, covalence, coordination, bond length, and crystal-field strength).[31,32] $Eu^{3+}$ emission is always in the red / orange region. The emission associated with $Eu^{3+}$, originating from 4f-4f transitions, is scarcely affected by the structure / crystal field because 4f-orbital electrons are well shielded by the outer orbital electrons.[28,33] The $Ce^{3+}$ dopant exhibits a bluish purple emission in LBSO (Figure S1), which originates from 4f-5d transitions.[33,34]

On the other hand, the $Ce^{4+}$ dopant exhibits no emission in LBSO (Figure S1). In this case, an appropriate ratio of $Eu^{2+}$, $Eu^{3+}$, and $Ce^{3+}$ can be expected to produce a white emission.

In the first step of the HT synthesis of phosphors, eight samples of LBSO doped with different amounts (molar ratio) of Eu and Ce (0.5%Ce; 0.5%Eu; 0.25%Eu and 0.25%Ce; 0.25%Eu and 0.5%Ce; 0.5%Eu and 0.25%Ce; 0.5%Eu and 0.5%Ce; 0.5%Eu and 0.75%Ce; 0.75%Eu and 0.5%Ce) were synthesized in Ar / $H_2$ (Experimental details in the section "Experimental procedures"). XRD patterns (Figure 1(a)) confirmed that the doped samples were pure (COD-2017068). The diffuse reflection spectra of single-doped LBSO with different activators oxidation state ($Eu^{2+}$, $Eu^{3+}$, $Ce^{3+}$, and $Ce^{4+}$) showed different characteristic bands for

each single-doped compound, confirming that the doping was successful (Figure 1(b)).

In the second step, 88 samples were prepared from the eight synthesized samples by oxidation of the dopants under a gradient of temperature (Table S1, Figure 2(a), Figure S2; Detailed synthetic process in the section "Experimental procedures"). During the oxidation of $x$ $Eu^{2+}$ into $x$ $Eu^{3+}$ and $y$ $Ce^{3+}$ into $y$ $Ce^{4+}$, $x+y$ lithium vacancies are produced to respect the charge balance.[33] PL spectra of LBSO:$Ce^{3+}$,$Eu^{2+}$ (Figure S3-S10) were recorded in a HT manner using a home-made XY robotic platform setup (see details in the section "Experimental procedures" and the supporting information). The CIE coordinates determined from the emission spectra of all 88 samples were shown in Figure 2(b). These coordinates covered bluish purple, green, yellow / green, orange, pink and white regions according to the KS A 0012 (2013) standard (Figure S11).[35] Among these samples, only few exhibited white emission showing that identifying the optimal conditions to isolate white phosphors was challenging. In addition, the identification and sorting of important experimental conditions as well as the statistic assessment of boundaries between emission colors (Figure 2(b) and Figures S3-S10) require the use of ML models.

In order to predict the emission color and better understand the underlying mechanism, ML was used to analyze the experimental data (SI, Figure S12-S13). Specifically, three experimental parameters considered as important by the chemists, i.e. (i) the total concentration of dopants [Eu] + [Ce], (ii) the ratio of the two dopants, $x$ = [Eu] / ([Eu] + [Ce]), and (iii) the temperature of oxidation, were used to build the model to predict the emission color. The results of the decision tree model can be seen in Figure 2(c), which shows only a small number of samples can show white emissions.

The results of the decision tree model can be summarized in the Figure 3(a). The ratio and the temperature of oxidation were the two experimental parameters selected by the decision tree model to predict the emission colors as the total amount of dopants do not have significant influence on the outcome. For this reason, the total amount of dopants does not appear in the decision tree (Figure 2(c)). Three regions of ratio $x$ ($x$ < 0.17, 0.17 < $x$ < 0.83, and $x$ > 0.83) could be further analyzed to rationalize the mechanisms of luminescence as a function of the temperature of oxidation.

When $x$ < 0.17 (Figure 3(a)), only bluish-purple emission originating from $Ce^{3+}$ was obtained irrespective of the temperatures of oxidation. The single doped LBSO:Ce is representative of this region. Figure S4 shows the PL spectra of this compound for different temperatures of oxidation. The emission of $Ce^{3+}$ decreases with temperature due to the oxidation of $Ce^{3+}$ into $Ce^{4+}$. However, no other emission is observed because $Ce^{4+}$ is not an emission center in LBSO. Thus, the emission color (bluish purple) is scarcely affected by the temperature of oxidation. Interestingly, when the concentration of Eu increases (i.e. $x$ > 0.17), the bluish-purple emission color is not observed due to an efficient ET between Ce and Eu (Figure 3(b)).

When $x$ > 0.83 (Figure 3(a)), $Ce^{3+}$ plays an insignificant role on emission colors. Thus, the emission color changes from green to orange with the temperature of treatment under air due to the progressive oxidation of $Eu^{2+}$ (green) into $Eu^{3+}$ (orange) (Figure S4).

When 0.17 < $x$ < 0.83 (Figure 3(a)), yellow green, white, pink, and orange luminescence could be obtained according to the temperature of oxidation. In this range of ratio $x$, the emission color is affected by (i) the oxidation of $Eu^{2+}$ and $Ce^{3+}$ activators and (ii) the ET from $Ce^{3+}$ to $Eu^{2+}$ / $Eu^{3+}$. The oxidation of $Eu^{2+}$ and $Ce^{3+}$ activators can be assessed by investigating the evolution of the emission intensities with the temperature for single doped LBSO:Eu and LBSO:Ce materials (i.e. the compounds without ET; Figure S3, Figure S4, Figure 3(c)). The oxidations of $Ce^{3+}$ into $Ce^{4+}$, and $Eu^{2+}$ into $Eu^{3+}$ occur from 605 °C to 800 °C and from 500 °C to 750 °C, respectively. On the other hand, the ET from $Ce^{3+}$ to Eu can be investigated through the analysis of spectral overlap (Figures 3(b) and Figure S14). Thus, a significant overlap can be observed between the emission spectrum of LBSO:Ce and the excitation spectra of LBSO:$Eu^{2+}$ / LBSO:$Eu^{3+}$ suggesting an efficient ET between Ce and Eu. In addition, the metal-to-metal charge transfer (MMCT) between $Ce^{3+}$ and $Eu^{3+}$ should be considered. The distance between dopants in our compounds is above 24.8 Å which is longer than the maximum distances between $Ce^{3+}$ and $Eu^{3+}$ for MMCT (typically 14 Å in oxide hosts) and ET (see equation in supporting Information),[36] [37] Thus, the MMCT and ET between $Ce^{3+}$ and $Eu^{3+}$ can be neglected. In this case, only the ET from $Ce^{3+}$ to $Eu^{2+}$ should be considered. To rationalize how the oxidation of dopants and the ET influence the emission colors in the range 0.17 < $x$ < 0.83, the co-doped LBSO:0.5%Eu,0.5%Ce ($x$ = 0.5) was considered for in-depth analysis. For this compound, four colors of emission corresponding to the combination of several contributions could be obtained according to the temperatures of oxidation, i.e., *Yellow green* from 385 °C to 628 °C (Figure 3(a)- *Zone 1*), *White* from 628 °C to 673 °C (Figure 3(a)- *Zone 2*), *Pink* from 673 °C to 783 °C (Figure 3(a)- *Zone 3*), and *Orange* above 783 °C (Figure 3(a)- *Zone 4*). To explain the origin of these colors of emissions, the intensity of the emission bands associated with $Ce^{3+}$, $Eu^{2+}$ and $Eu^{3+}$ ions can be followed (Figures 3(d) and Figure S8). In *Zone 1* (T < 628 °C; Figures 3(a) and Figure 3(d)), the oxidation of $Eu^{2+}$ into $Eu^{3+}$ occurs while $Ce^{3+}$ is not oxidized (Figure 3(d)). The intensity of $Ce^{3+}$ remains very low due to an efficient ET from $Ce^{3+}$ to $Eu^{2+}$. A yellow green color of the emission can be observed originating mainly from $Eu^{2+}$ (green) with small contributions of $Eu^{3+}$ (orange) without $Ce^{3+}$ (bluish purple). In *Zone 2* (628 °C < T < 673 °C; Figures 1d and Figure 3(d)), $Eu^{2+}$ is strongly oxidized into $Eu^{3+}$ while $Ce^{3+}$ is slightly oxidized into $Ce^{4+}$ (Figure 3(c)). The ET from $Ce^{3+}$ to $Eu^{2+}$ decreases with the oxidation of $Eu^{2+}$ into $Eu^{3+}$. Such phenomenon results in the increase of the intensity of emission associated with $Ce^{3+}$. Thus, the white color of the emission results from the contributions of $Eu^{2+}$ (green), $Ce^{3+}$ (bluish purple) and $Eu^{3+}$ (orange). In *Zone 3* (673 °C < T < 783 °C; Figures 3(a) and Figure 3(d)), $Eu^{2+}$ and $Ce^{3+}$ are oxidized into $Eu^{3+}$ and $Ce^{4+}$, respectively.

The oxidation of $Eu^{2+}$ into $Eu^{3+}$ leads to a decrease of ET from $Ce^{3+}$ to $Eu^{2+}$ which should result in the increase of the bluish-purple emission from $Ce^{3+}$. However, this increase of emission is compensated by the oxidation of $Ce^{3+}$ into $Ce^{4+}$. For this reason, the intensity of emission associated with $Ce^{3+}$ shows no change when compared with *Zone 2*. Thus, a pink color of the emission can be observed due to the presence of $Eu^{3+}$ (orange) and $Ce^{3+}$ (bluish purple) and the absence of $Eu^{2+}$ (green). In *Zone 4* (T > 783 °C; Figures 3(a) and Figure 3(d)), $Eu^{2+}$ and $Ce^{3+}$ ions are fully oxidized into $Eu^{3+}$ and $Ce^{4+}$. Thus, the orange color of the emission originates from only $Eu^{3+}$ (orange).

## CONCLUSION

A HT experimental approach combined with ML was reported to discover single-phase white phosphors and predict the

emission color for inorganic materials with multiple activators. This strategy was demonstrated with the investigation of LBSO:Eu,Ce system. The key experimental parameters enabling white emission were identified and the energy transfers between activators could be rationalized. We believe such a ML based approach could also be of interest for other physical properties such as magnetism, photocatalysis, or conductivity for which the control of dopants oxidation states can greatly influence the functionalities. More generally, adopting ML tools to appropriately sort the experimental data and better select the experimental conditions could become a very efficient strategy to accelerate the discovery of new materials. The generalization of some standardized experimental files for the synthesis of materials (e.g. on the model of *Crystallographic Information Files* for the crystal structures), would be of great importance for this adoption of ML tools which requires well organized and representative datasets.

## EXPERIMENTAL PROCEDURES

**Samples preparation:** $BaCO_3$ (VWR, 99%), $SiO_2$ (Alfa Aesar, 99.99%), $Li_2CO_3$ (Alfa Aesar, 99.99%), $CeO_2$ (Alfa Aesar, 99.99%) and $Eu_2O_3$ (Alfa Aesar, 99.99%) were used as starting materials. $Li_2BaSiO_4:Eu_x,Ce_y$ (LBSO:Eu,Ce) (with x and y varying from 0.25 to 0.75mol% /nominal ratios) powder samples were prepared via a solid-state reaction process. A 5mol% excess of the $Li_2CO_3$ was used due to its high vaporization during heating, while other raw materials were weighted based on their stoichiometric ratio. The powders were mixed and then transferred to an alumina crucible. The mixture was heated at 550˚C with a temperature increase rate of 100˚C/h. After 1 h at 550°C, the temperature was increased up to 810˚C at the same rate. The samples were kept at this temperature for 6 h and then cooled to room temperature with a rate of 150˚C/h. For LBSO doped with $Ce^{3+}$ and/or $Eu^{2+}$, the mixture should be heated in a reducing atmosphere (95% Ar, 5% $H_2$) with a flow rate of 30 cc/min, while LBSO doped with $Ce^{4+}$ and/or $Eu^{3+}$ were synthesized in air.

**Controlled oxidation of dopants:** A series of samples LBSO:$Ce^{3+}$, $Eu^{2+}$ with different concentrations of the Eu ions and the Ce ions (0.5mol%Ce; 0.5mol%Eu; 0.25mol%Eu and 0.25mol%Ce; 0.25mol%Eu and 0.5mol%Ce; 0.5mol%Eu and 0.25mol%Ce; 0.5mol%Eu and 0.5mol%Ce; 0.5mol%Eu and 0.75mol%Ce; 0.75mol%Eu and 0.5mol%Ce) were synthesized in $Ar/H_2$ and then placed in a sample holder machined in Stumatite ceramic. The samples with 8 different concentrations of dopants were placed in different rows, each row corresponds to the same concentration (11 boxes for each row). Then the sample holders were placed under a gradient of temperature in air for 2h (STEP 1 in Schematic S1). The temperature treatment was in the range from 385 °C to 795 °C (the temperature of each position is reported in Table S1). Finally, the emission color could be observed under UV lamp (λ = 254 nm) (STEP 2 in Schematic S1). The controlled synthesis temperature can be performed simply using a tube furnace available in all solid-state chemistry laboratory (such tube furnace exhibits a gradient of temperature between the center and the extremities).

**Data collection:** The photoluminescence (PL) spectra of $Li_2BaSiO_4:Ce^{3+},Eu^{2+}$ after HT approach, were recorded in a high-throughput manner using a home-made XY robotic platform setup (Schematic S2). The sample holder was placed on the XY table, which can move along two axes controlled by computer. Thus, each sample will be characterized by simply moving step by step the XY axes of the platform in order to automatically change the analyzed sample.

**Machine-learning:** The decision tree model was performed in this study due to its intuitive, interpretable, and easy to visualize nature. The model was developed using the data obtained by the HT approach. The raw data contained 88 samples (dataset in SI – the eight initial samples are represented in different colors in this dataset). The main idea was to explore a “general” mechanism that can inform the color of the materials obtained from experiments. We retained 20% random samples of the raw data for external validation purpose, assuming those data would be from future new experiments. The random sampling was carried out using the function createdatapartition in R package {caret} (R version 3.6.2; R codes are attached in a separate file, named as DecisionTree_clean.Rmd), with an attempt of balancing the color class distributions within the splits. Thus, this random sampling was realized within each color group, rather than sampling over all the data. The tree model was established on the remaining 80% of the raw data, using the function rpart in R package {rpart}. The cross validation has been used inside rpart to obtain the best tree that could sufficiently describe the data with the minimal model complexity. The overall accuracy (calculated as (number of correct prediction) / (total number of samples in the dataset) was 88.9% on the modeling data-cut (i.e., the 80% of the raw data) and 87.5% on the validation data-cut (i.e., 20% of the raw data). The accuracy per color is summarized in the table S2. In order to qualify the built tree, asserting the level of precision one can expect from it, we performed the 5-fold cross-validation. Specifically, the raw data was split into 5 folds, using the createFolds function in R package {caret} and balancing the color class distributions between folds. The tree model was built on any 4 folds (using the same rpart function as in the original model) and tested on the 5th fold. Thus, 5 models were obtained after performing once 5-fold cross-validation. By repeating the 5-fold cross-validation process for 100 times, we obtained in total 500 decision tree models. And we confirmed that the decision tree performed quite well with the 5-fold average accuracy as 83.2% on the test fold and 89.9% on the training folds. The results from cross-validation showed that the size of the raw data was sufficient for this study. The accuracy of each of the 100 5-fold cross-validation exercises is shown in a separate file (named as accuracy_5-fold-cross-validation.xlsx).

Usually, larger data size can assist in refining the model when exploring the underlying mechanism. As a sensitivity analysis, we built a tree model using all the 88 samples (i.e., without random split of the raw data) using the same rpart function. The overall accuracy was 89.8% which is very similar to the original approach. The obtained tree was shown in Figure S12 and summarized in Figure S13.

**Characterization:** Phase identification was performed using an X-ray diffractometer (D8 Bruker) with Cu Kα radiation. Diffuse reflection spectra were acquired using a Perkin lambda 1050 equipped with a 150 mm integrating sphere. The photoluminescence (PL) and photoluminescence excitation (PLE) spectra were carried out using a spectrofluorometer Fluorolog-3 from Horiba equipped with a 450 W Xe light source.

## ACKNOWLEDGEMENTS

This work was supported by the National Agency for Research (ANR Young Researchers, ANR-16-CE08-0003-01, Combi-SSL project) and Region Pays de la Loire (Etoiles montantes en Pays de la Loire 2017, project “Découverte de pérovskites hybrides

assistée par ordinateur"). The National Natural Science Foundation of China (51472188, 51521001, and 51872217), Natural Research Funds of Hubei Province (No. 2016CFB583), the Fundamental Research Funds for the Central Universities in China and the "111" project (B13035). HL Yuan thanks the China Scholarship Council (CSC) for fellowship support.

## AUTHOR CONTRIBUTIONS

H. Yuan and R. Gautier designed the study. H. Yuan performed the sample preparation. H. Yuan conducted sample measurements and characterizations with contributions from other authors. L. Qi conducted the machine-learning under the discussion with H. Yuan and R. Gautier. H. Yuan wrote the paper with contributions from all authors.

## DECLARATION OF INTERESTS

The authors declare no competing interests.

**Keywords:** Single-phase white phosphor • Oxidation • Machine learning • Decision tree

## REFERENCES

[1] L. Wang, R.-J. Xie, T. Suehiro, T. Takeda, N. Hirosaki, *Chemical reviews* **2018**, *118*, 1951.
[2] F. G. Montoya, A. Peña-García, A. Juaidi, F. Manzano-Agugliaro, *Energy and buildings* **2017**, *140*, 50.
[3] E. F. Schubert, J. K. Kim, *Science* **2005**, *308*, 1274.
[4] H. Zhu, C. C. Lin, W. Luo, S. Shu, Z. Liu, Y. Liu, J. Kong, E. Ma, Y. Cao, R.-S. Liu, *Nature communications* **2014**, *5*, 1.
[5] M. Jia, J. Wen, W. Luo, Y. Dong, F. Pang, Z. Chen, G. Peng, T. Wang, *Journal of Luminescence* **2020**, *221*, 117063.
[6] G. Blasse, A. Bril, *Applied Physics Letters* **1967**, *11*, 53.
[7] G. Li, Y. Tian, Y. Zhao, J. Lin, *Chemical Society Reviews* **2015**, *44*, 8688.
[8] D. Singh, C. Basu, M. Meinhardt-Wollweber, B. Roth, *Renewable and Sustainable Energy Reviews* **2015**, *49*, 139.
[9] B. Shao, J. Huo, H. You, *Advanced Optical Materials* **2019**, *7*, 1900319.
[10] H. Zhu, X. Liu, R. Fu, Y. Shi, H. Wang, Q. He, X. Song, *Journal of Luminescence* **2019**, *211*, 1.
[11] P. Pust, V. Weiler, C. Hecht, A. Tücks, A. S. Wochnik, A.-K. Henß, D. Wiechert, C. Scheu, P. J. Schmidt, W. Schnick, *Nature materials* **2014**, *13*, 891.
[12] L. Liu, L. Wang, C. Zhang, Y. Cho, B. Dierre, N. Hirosaki, T. Sekiguchi, R.-J. Xie, *Inorganic chemistry* **2015**, *54*, 5556.
[13] M. M. Rodríguez-García, J. G. Williams, I. R. Evans, *Journal of Materials Chemistry C* **2019**, *7*, 7779.
[14] H. Yuan, F. Massuyeau, N. Gautier, A. B. Kama, E. Faulques, F. Chen, Q. Shen, L. Zhang, M. Paris, R. Gautier, *Angewandte Chemie* **2020**, *132*, 2824.
[15] S. A. Khan, Z. Hao, H. Wei-Wei, L.-Y. Hao, X. Xu, N. Z. Khan, S. Agathopoulos, *Journal of Materials Science* **2017**, *52*, 10927.
[16] D. Wen, H. Kato, M. Kobayashi, S. Yamamoto, M. Mitsuishi, M. Kakihana, *Journal of Materials Chemistry C* **2017**, *5*, 4578.
[17] M. Shang, C. Li, J. Lin, *Chemical Society Reviews* **2014**, *43*, 1372.
[18] X. Zhang, Z. Zhu, Z. Guo, Z. Sun, Z. Yang, T. Zhang, J. Zhang, Z. Wu, Z. Wang, *Inorganic Chemistry Frontiers* **2019**, *6*, 1289.
[19] R. Gautier, X. Li, Z. Xia, F. Massuyeau, *Journal of the American Chemical Society* **2017**, *139*, 1436.
[20] M. L. Nisbet, I. M. Pendleton, G. M. Nolis, K. J. Griffith, J. Schrier, J. Cabana, A. J. Norquist, K. R. Poeppelmeier, *Journal of the American Chemical Society* **2020**.
[21] Y. Xie, C. Zhang, X. Hu, C. Zhang, S. P. Kelley, J. L. Atwood, J. Lin, *Journal of the American Chemical Society* **2019**.
[22] P. Raccuglia, K. C. Elbert, P. D. Adler, C. Falk, M. B. Wenny, A. Mollo, M. Zeller, S. A. Friedler, J. Schrier, A. J. Norquist, *Nature* **2016**, *533*, 73.
[23] L. Dong, L. Zhang, Y. Jia, B. Shao, W. Lu, S. Zhao, H. You, *ACS Sustainable Chemistry & Engineering* **2020**.
[24] Z. Wang, B. Wang, Y. Liu, Z. Huang, *Materials Research Express* **2019**, *6*, 115903.
[25] G. Kaur Behrh, H. Serier-Brault, S. Jobic, R. Gautier, *Angewandte Chemie International Edition* **2015**, *54*, 11501.
[26] R. Génois, S. Jobic, G. Ouvrard, F. Massuyeau, R. Gautier, *Applied Materials Today* **2020**, *20*, 100643.
[27] Y. Pan, X. Xie, Q. Huang, C. Gao, Y. Wang, L. Wang, B. Yang, H. Su, L. Huang, W. Huang, *Advanced Materials* **2018**, *30*, 1705256.
[28] Q. Y. Zhang, K. Pita, W. Ye, W. X. Que, *Chemical physics letters* **2002**, *351*, 163.
[29] H. Liao, M. Zhao, M. S. Molokeev, Q. Liu, Z. Xia, *Angewandte Chemie* **2018**, *130*, 11902.
[30] Q. Zhang, X. Wang, X. Ding, Y. Wang, *Inorganic chemistry* **2017**, *56*, 6990.
[31] H. He, R. Fu, X. Zhao, X. Song, Z. Pan, S. Zhang, Z. Deng, Y. Cao, *Electrochemical and Solid-State Letters* **2010**, *13*, J21.
[32] T. Kobayasi, S. Mroczkowski, J. F. Owen, L. H. Brixner, *Journal of Luminescence* **1980**, *21*, 247.
[33] M. Xie, C. Luo, *physica status solidi (RRL)–Rapid Research Letters* **2012**, *6*, 412.
[34] W. Ying, T. Yusufu, N. Sujian, A. Sidike, in *Asia Communications and Photonics Conference*, Optical Society Of America, **2017**, pp. Su2A-112.
[35] K. Choi, J. Lee, H.-J. Suk, *Applied ergonomics* **2016**, *52*, 222.
[36] G. Blasse, *Journal of Solid State Chemistry* **1986**, *62*, 207.
[37] A. A. Setlur, *Electrochemical and Solid State Letters* **2012**, *15*, J25.

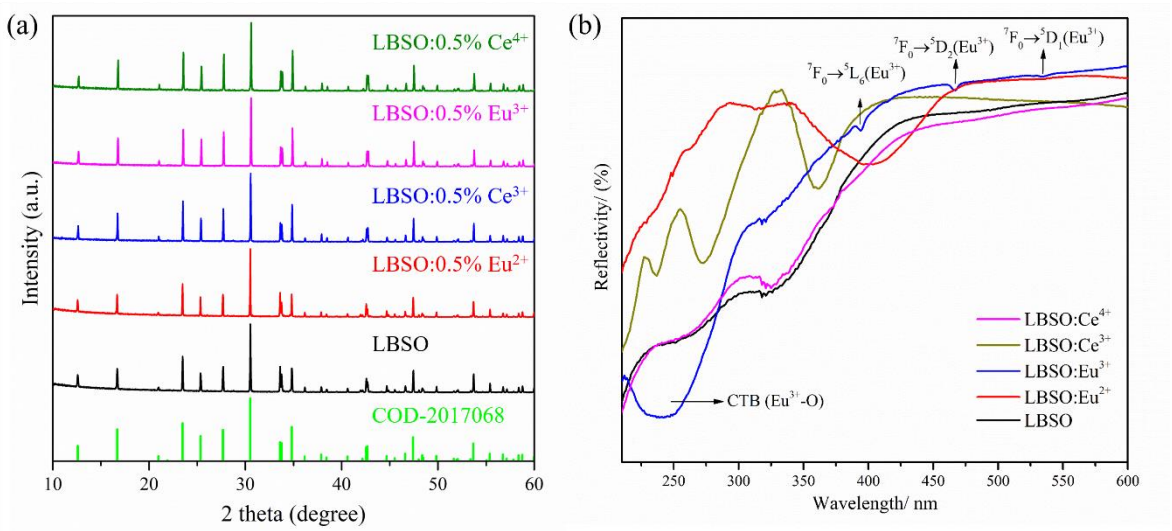


Figure 1 (a) Powder X-ray diffraction (PXRD) patterns of LBSO, LBSO:$Eu^{2+}$, LBSO:$Eu^{3+}$, LBSO:$Ce^{3+}$, and LBSO:$Ce^{4+}$; (b) Diffuse reflection spectra of LBSO (black), LBSO:$Eu^{2+}$ (red – the band centered at 405 nm originates from $4f^7 \rightarrow 4f^6 5d^1$ transition), LBSO:$Eu^{3+}$ (blue – the band centered at 240 nm belongs to the charge-transfer band (CTB) of $Eu^{3+}$-O, peaks from 390 nm to 550 nm belong to $^7F_0 \rightarrow {}^5D_1$, $^7F_0 \rightarrow {}^5D_2$, $^7F_0 \rightarrow {}^5L_6$), LBSO:$Ce^{3+}$ (green – the peaks centered at 237 nm, 272 nm, and 360 nm correspond to the $4f^1 \rightarrow 4f^0 5d^1$ transitions, LBSO:$Ce^{4+}$ (pink – the band centered at 325 nm belongs to the CTB of $Ce^{4+}$-O).

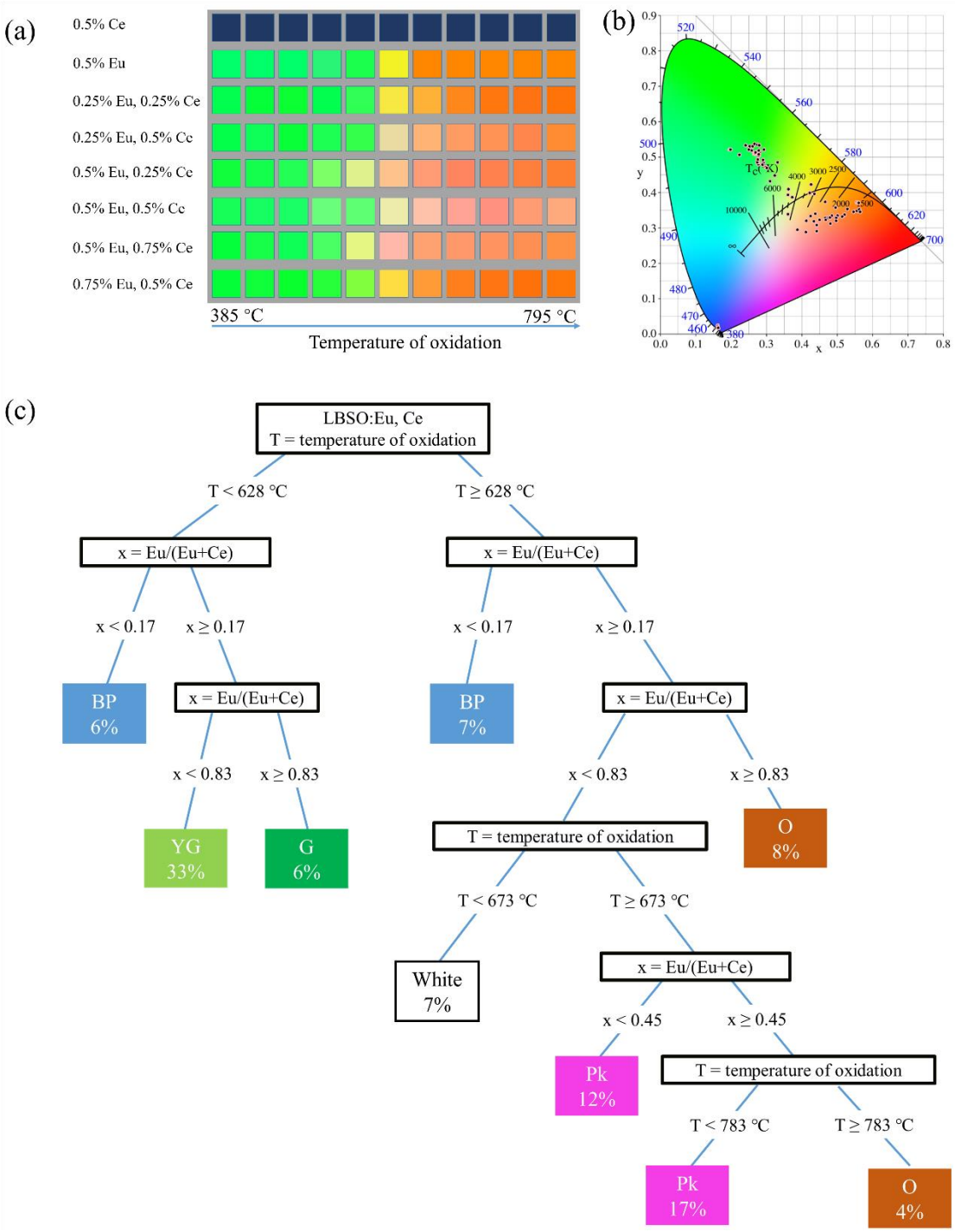


Figure 2 (a) 88 samples prepared from the eight synthesized samples by oxidation of the dopants under a gradient of temperature (the colors were simulated using the CIE coordinates calculated from the emission spectra of each sample); (b) The CIE of all 88 samples; (c) Decision tree classification of emission colors (T: oxidation temperature; BP: bluish-purple; YG: yellow green; G: green; Pk: pink; O: orange); the percentages of training samples associated to each leave are provided (more details can be found in the SI: DecisionTree_clean.Rmd).

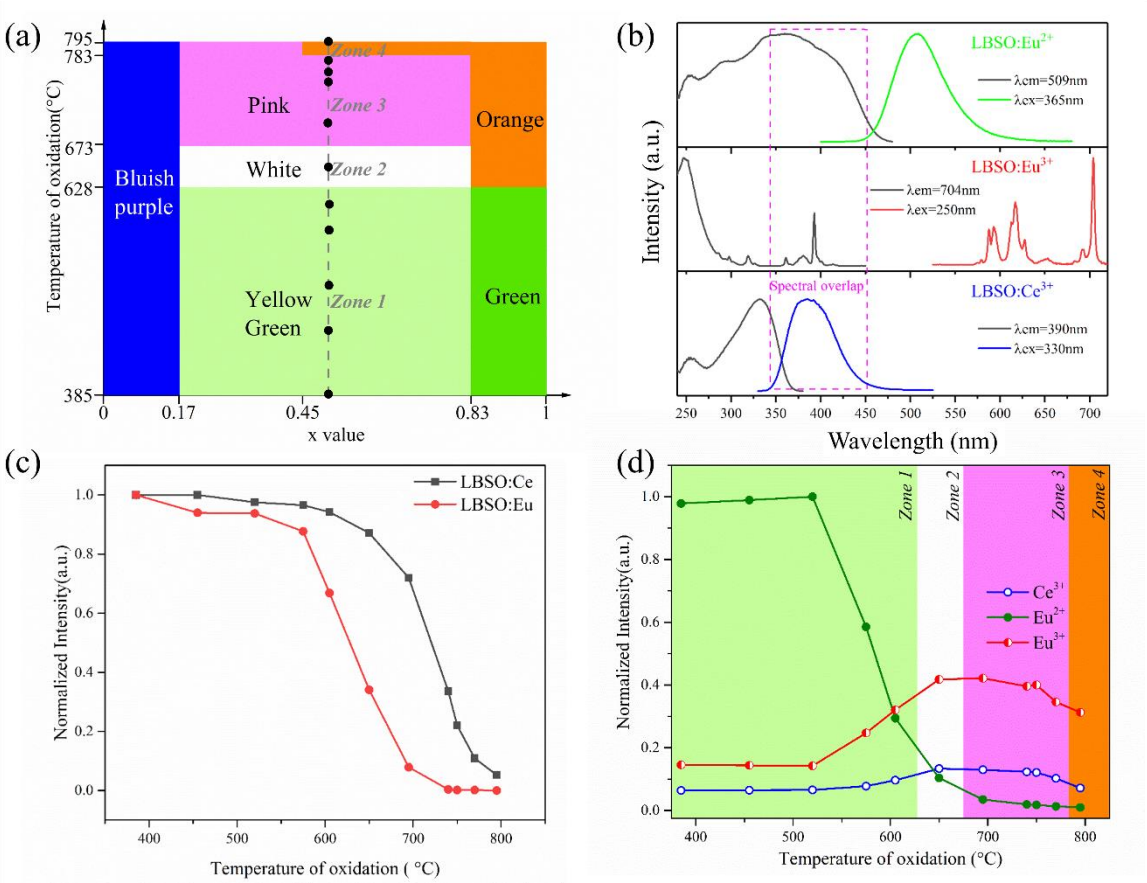


Figure 3 (a) Results of decision tree model based on the 88 samples (x = [Eu]/([Ce]+[Eu])). The black dots correspond to the experimental conditions of the samples set LBSO:0.5%Eu,0.5%Ce (x = 0.5). For this sample, four zones of emission colour (Zone 1: Yellow green, Zone 2: White, Zone 3: Pink, Zone 4: Orange) are obtained according to the temperature of oxidation (black dot); (b) PL and PLE spectra of the LBSO:$Eu^{2+}$, LBSO:$Eu^{3+}$ and LBSO:$Ce^{3+}$ samples; (c) Evolution of the emission intensity of $Eu^{2+}$ ($\lambda_{em}$ = 510 nm) and $Ce^{3+}$ ($\lambda_{em}$ = 400 nm) in LBSO:Eu and LBSO:Ce with the oxidation temperature; (d) Evolution of the emission intensities associated with $Ce^{3+}$ ($\lambda_{em}$ = 400 nm, blue line), $Eu^{2+}$ ($\lambda_{em}$ = 510 nm, green line), and $Eu^{3+}$ ($\lambda_{em}$ = 704 nm, red line) vs. the temperature of oxidation for LBSO:0.5%Eu, 0.5%Ce. All the intensities of the emissions are normalized to the maximum intensity ($Eu^{2+}$ emission of the sample oxidized at 520 °C).